Colloid Polym Sci (2006) 285: 27–37
DOI 10.1007/s00396-006-1527-2

ORIGINAL CONTRIBUTION

Chiranjeevi Peetla
Karlheinz Graf
Jörg Kressler

Langmuir monolayer and Langmuir–Blodgett films of amphiphilic triblock copolymers with water-soluble middle block

Received: 16 November 2005
Accepted: 4 June 2006
Published online: 26 July 2006

C. Peetla · J. Kressler (✉)
Department of Chemistry,
Institute of Physical Chemistry, Martin Luther University Halle-Wittenberg,
06099 Halle (Saale), Germany
e-mail: joerg.kressler@iw.uni-halle.de
Fax: +49-345-5527017

K. Graf
Max Planck Institute for Polymer Research,
Ackermannweg 10,
55128 Mainz, Germany

Abstract Langmuir monolayers and Langmuir–Blodgett (LB) film morphology of amphiphilic triblock copolymers are studied using surface pressure-area measurements and atomic force microscopy (AFM), respectively. The triblock copolymers are composed of long water-soluble poly(ethylene oxide) (PEO) chains as middle block with very short poly (perfluorohexylethyl methacrylate) (PFMA) end blocks. The surface pressure-area isotherms show phase transitions in the brush regime. This phase transition is due to a rearrangement of PFMA block at the air–water interface. It becomes more significant with increasing PFMA content in the copolymer. LB films transferred at low surface pressures from the air–water interface to hydrophilic silicon substrates show surface micelles in the size range of 50–100 nm. A typical crystalline morphology of the corresponding PEO homopolymer is observed in LB films of copolymers with very short PFMA blocks, transferred in the brush region at high surface pressure. This crystallization is hindered with increasing PFMA content in the copolymer.

Keywords Langmuir monolayers · Langmuir–Blodgett films · Surface micelles

Introduction

Block copolymers are usually composed of mutually immiscible blocks. They are known to form self-assembled nanostructures of various morphologies in the presence of selective solvents and surfaces [1, 2]. In particular, ordered structures of thin block copolymer films on solid surfaces are of considerable scientific interest as well as for their potential applications [3]. Such ordered structures can be obtained with the well-established Langmuir–Blodgett (LB) technique by transferring amphiphilic molecules from the water surface to solid substrates [4]. This technique has the advantage of controlling the molecular density and thus the phase behavior of the monolayer.

Numerous groups have reported on the monolayer behavior of amphiphilic block copolymers anchored at the air–water interface by neutron reflectivity [5, 10], by light scattering studies [6], and by measuring the surface pressure vs the mean molecular area (π–mmA) at constant temperature, i.e., the surface isotherms, particularly for poly(ethylene oxide)-*block*-poly(styrene) (PEO-*b*-PS)-based linear diblock [5–19] and star block copolymer systems [20–23]. In general, a characteristic rearrangement occurs with compression of the monolayer of block copolymers containing PEO as a hydrophilic block. Typically, the Langmuir isotherms show three distinct regions with one phase transition. This phase transition was interpreted according to scaling theories of Alexander [24] as the formation of pancake-like structures at large molecular areas transforming into brushes at lower molecular areas with an intermediate plateau region corresponding to the dissolution of the PEO block. In contrast, in isotherms of PS-*b*-PEO with high PS content, the intermediate plateau region was reduced significantly [15] or completely disappeared [16, 19]. For telechelic PEO copolymer systems, Barentin et al. [25] have reported a phase transition in the brush regime in addition to the described phase transition. This transition was attributed to

the dissolution of alkyl chains resulting in the loss of polymer into the subphase. Multiple transitions were observed in poly(styrene)-*block*-poly(alkyl acrylate) diblock copolymer monolayers.

Additionally, micelles were observed in anchored amphiphilic block copolymer chains after the transfer to a solid substrate by transmission electron microscopy, TEM, and atomic force microscopy, AFM [26–33]. Surface micelle formation and aggregation at the air–water interface was found for PS-*b*-PEO linear diblock copolymer [14–18] for three-arm star block copolymer [20, 22, 23] and for hetero-arm star block copolymer [21] systems after the transfer at various surface pressures. Well-organized structures developed when the microphase segregation of the polymer was driven through the choice of solvent and grafting density on the solids as a result of different initial surface pressures [34]. Three different mechanisms were reported to explain the domain formation in linear amphiphilic block copolymers after transfer from the liquid surface to the solid. According to Goncalves da Silva et al. [11], block copolymers form micelles in the spreading solution already. Upon spreading, they form surface micelles, which become more densely packed with increasing surface pressure. In contrast, An et al. [35] and Israelachvili [36] suggested that the polymers were spread as unimers onto the subphase and aggregated upon compression. Cox et al. [16] stated that linear block copolymers deposit as a combination of both models. The different models, suggested for the formation of surface micelles, reflect the richness of block copolymers under investigations. To get a deeper insight into the interrelation between micelle formation and pancake-to-brush transition, the length of the anchor relative to the polymer block has to be changed systematically.

In this paper, we report on the phase behavior of monolayers from amphiphilic triblock copolymers of PEO and poly(perfluorohexylethyl methacrylate) (PFMA) at the air–water and the air–silicon interfaces. Compared to the previously described systems, they contain a long hydrophilic middle block (PEO) with very short hydrophobic end blocks (PFMA). The PFMA block consists of a methacrylate backbone with nonfluorinated ethyl and perfluorinated *n*-hexyl side chains. These block copolymers are highly surface active and form micelles and clusters in aqueous solutions [37]. A clear aqueous solution is formed only when the hydrophobic PFMA part is less than 15 wt% [37, 38]. The phase behavior at the air–water interface was studied by means of Langmuir isotherms. The resulting morphology of the monolayers was investigated by AFM after the transfer to silicon wafers at different surface pressures. The PFMA block chain length was varied to study the influence on the brush formation in Langmuir monolayers and on the surface morphology of the LB films.

Experimental section

Materials

PFMA-*b*-PEO-*b*-PFMA triblock copolymers used in this study (see Fig. 1) were synthesized and characterized in accordance to the previously reported procedure [39]. The molecular properties of the block copolymers are presented in Table 1. In the abbreviation scheme PEO_xF_y, x represents the molar mass of PEO in kilograms per mole and y represents the PFMA content in weight percent in the block copolymer. For instance, $PEO_{20}F_4$ is a triblock copolymer with 4 wt% PFMA in the outer blocks and a PEO middle block of 20 kg·mol^{-1}. The PEO molar masses are according to the supplier. These PEO samples were converted into a macroinitiator, and the PFMA blocks were added [39]. The obtained M_n values are based on size exclusion chromatography data where the calibration is carried out using PEO standards. Comparing the block copolymers with pure PEO samples, the obtained masses are too low. For example, $PEO_{10}F_9$ has a molar mass of 9.4 kg mol^{-1} whereas the PEO middle block has a molar mass of 10 kg mol^{-1}. This is a result of the decreased hydrodynamic volume due to the presence of fluorine containing blocks [39].

Surface pressure measurements

The surface isotherms of the copolymers at the air–water interface, i.e., the plots of pressure (π) vs the mean molecular area (mmA), were measured with a Teflon® Langmuir trough system (KSV, Helsinki, Finland) equipped with two moving barriers and a microroughened platinum Wilhelmy plate. The maximum available surface area of the Langmuir trough is 76,800 mm^2 (compression ratio 8:1). As subphase, distilled water was used, which was subsequently passed through a water purification system from Purelab option system (ELGA, Celle, Germany) equipped with an organic removal cartridge (conductance 0.06 μS cm^{-1}). The purity of the bare water surface was checked before each measurement by a maximum compression ($\Delta\pi$<0.1 mN m^{-1}). The temperature of the water subphase was maintained at 23±0.5 °C

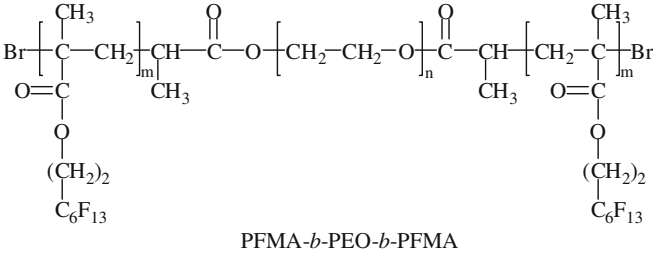

Fig. 1 Chemical structure of PFMA-*b*-PEO-*b*-PFMA triblock copolymer

Table 1 Molecular characteristic of copolymers

Copolymer	M_n[a] (kg mol^{-1})	PFMA[b] (wt%)	M_w/M_n
$PEO_{10}F_9$	9.4	9	1.33
$PEO_{10}F_{13}$	9.7	13	1.27
$PEO_{20}F_4$	27.2	4	1.4
$PEO_{20}F_9$	26.5	9	1.3
$PEO_{20}F_{13}$	26.7	13	1.2

[a]SEC results from THF using PEO standards
[b]^{1}H NMR results

using a circulating water bath system. Copolymers were dissolved (2 mg ml^{-1}) in HPLC grade chloroform (Sigma-Aldrich, Fluka, Seelze, Germany), and predetermined amounts were spread evenly on the subphase in 1–2 μl small drops using a Hamilton's digital microsyringe. The compression at a constant rate of 7.5 cm^2 min^{-1} was started after 20 min to ensure the full evaporation of solvent. To obtain the complete isotherm, the copolymer solutions were spread upon different initial pressures and thus different parts of the isotherm were recorded. After copying into one plot, they overlap within the experimental error. The experimental setup was enclosed in a box for constant humidity and minimization of surface contamination.

Substrate cleaning for Langmuir–Blodgett deposition

Silicon (111) wafers were cut into 3×1 cm substrates. They were cleaned using a modified Shiraki technique [40]. The silicon substrates were placed in a solution containing 4:1:1 (volume) $H_2O/H_2O_2/NH_4OH$ at 80 °C for 5 min, then rinsed in deionized water followed by washing at room temperature in a solution containing 3:1 H_2O/HF, and finally rinsed again in deionized water to remove residuals. This treatment resulted in a hydrophobic surface. Afterward, they were heated in a solution containing 5:1:1 (volume) H_2O/H_2O_2/HCl to 80 °C for 5 min. After cooling, they were rinsed in deionized water. The procedure was repeated with a dilute HF treatment until a contact angle with pure water of approximately 10° was achieved. The contact angle was measured optically with OCA 20 (DataPhysics, Filderstadt, Germany). The cleaned substrates were stored under double-distilled water until use. For LB film preparation, cleaned substrates were immersed into the subphase before the monolayer deposition. The monolayer was compressed until the desired transfer surface pressure was reached, then allowed to equilibrate for 10 min. The monolayers were transferred onto the silicon substrates at constant surface pressure by a vertical upstroke through the film at a constant rate of 1 mm min^{-1} (hydrophilic transfer).

Atomic force microscopy (AFM)

The transferred films were allowed to dry in air for at least 24 h in a desiccator at room temperature. LB film surface morphology was studied using a Nanoscope Multimode AFM in tapping mode (Digital Instruments, Santa Barbara, CA, USA). The silicon cantilevers (NSC15/AlBS/15 μMasch, Spain) were 125 μm long with a resonance frequency of approximately 325 Hz and a tip radius <10 nm (force constant 40 N m^{-1}). The images were captured with lateral scan frequency of 1–2 Hz and a set point ratio of 0.95. The acquired images were flattened using a second-order flattening routine in digital instrument software. The images from three different LB films for each sample were comparable, indicating reproducible depositions.

Results and discussion

Monolayer behavior at the air–water interface

Figure 2 shows compression isotherms obtained for triblock copolymers with a low PFMA content, $PEO_{10}F_9$ and $PEO_{20}F_4$. The isotherms are similar to the isotherms of PS-*b*-PEO diblock copolymers with a low PS content [7, 9, 10]. They show three different regimes. At high mmA, the surface pressures increase gradually with compression. For $PEO_{10}F_9$ and $PEO_{20}F_4$, the first increase of the surface pressure is observed at mmA of approximately 160 and 320 nm^2, respectively. With further compression, a pseudoplateau is observed at about 35 nm^2 and 8.4 mN m^{-1} or 70 nm^2 and 9.2 mN m^{-1}, respectively, where the surface pressure changes only slightly (8–10 mN m^{-1}). When compressed beyond the pseudoplateau, the surface pressure sharply increases until the film collapses at small mmA.

The isotherms for $PEO_{10}F_9$ and $PEO_{20}F_4$ reflect the typical behavior of anchored PEO chains at the air–water interface. At low surface pressures, a typical liquid-expanded monolayer is observed, where the hydrophobic PFMA segment anchors the polymer chain to the surface, while the PEO adopts a flattened conformation at the interface due to its affinity to the water. According to Alexander, this phase can be described as a self-similar adsorbed layer or as pancake-like [24]. The shift of the isotherms to larger areas with an increasing PEO block length confirms the adsorption of PEO blocks at the air–water interface. As the film is compressed laterally, the surface pressure increases due to an increased surface density of PEO blocks. In the pseudoplateau, the PEO blocks extend into the subphase forming brushes. As a confirmation, the plateau coincides with the pseudoplateau reported for homopolymer PEO systems [25]. The height of the plateau is slightly dependent on the molar mass of the PEO chains. The same behavior was observed for PEO-*b*-PS copolymers with different PEO block lengths by

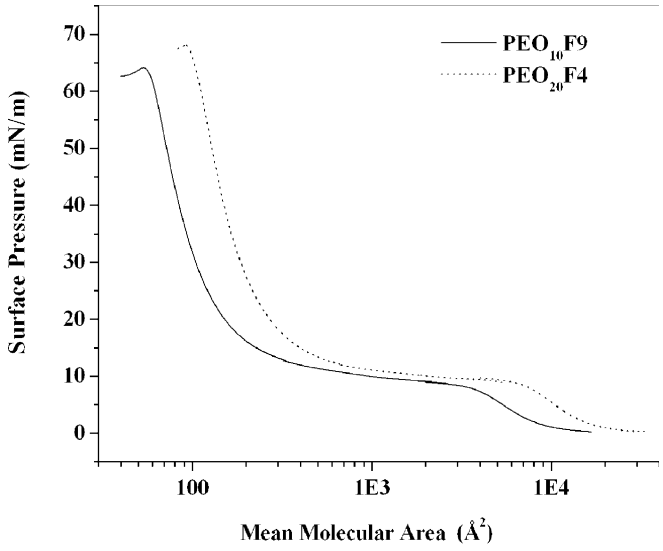

Fig. 2 Surface pressure (π)-mean molecular area (mmA) isotherms of $PEO_{10}F_9$ and $PEO_{20}F_4$. The collapse area is 56 Å^2 for $PEO_{10}F_9$ and 90 Å^2 for $PEO_{20}F_4$. A pseudoplateau is observed at 8.4 mN m^{-1} for $PEO_{10}F_9$ and at 9.2 mN m^{-1} for $PEO_{20}F_4$. *X*-axis log scaled

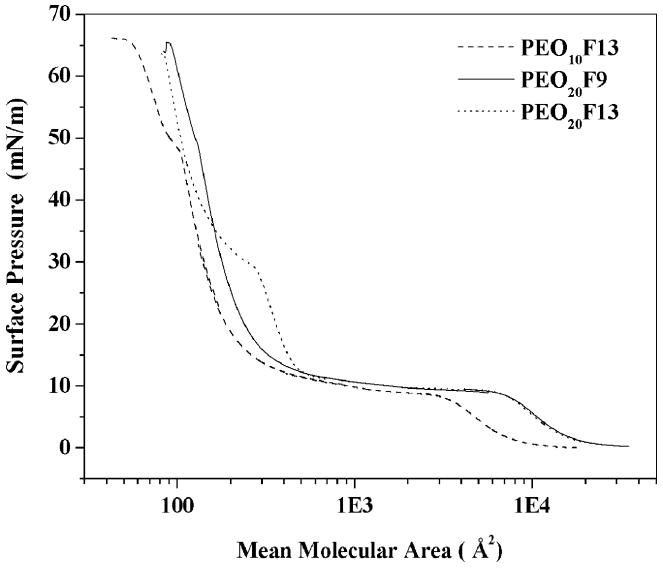

Fig. 3 Surface pressure (π)-mean molecular area (mmA) isotherms of $PEO_{10}F_{13}$, $PEO_{20}F_9$, and $PEO_{20}F_{13}$. A change in the slope is apparent at surface pressures of ~47, ~47, and ~30 mN m^{-1}, respectively. This transition corresponds to mmA of 101, 131, and 265 Å^2, respectively. *X*-axis log scaled

Goncalves da Silva et al. [7]. This plateau is indicative of a first-order pancake-to-brush transition and continued until either the PEO chains reached their limiting brush density or the anchoring block at the surface began to overlap, resulting in the dissolution of PEO into the subphase. In both cases, the sharp increase of the surface pressure beyond the plateau indicates the brush regime.

Figure 3 shows isotherms of the more hydrophobic block copolymers with a higher PFMA content, i.e., for $PEO_{10}F_{13}$, $PEO_{20}F_9$, and $PEO_{20}F_{13}$. The surface isotherms show two pseudoplateaus. The one at large mmA is comparable to the phase transition observed for the isotherms of copolymers with low PFMA content. Thus, it can be assigned to a pancake-to-brush transition. The limiting brush density, i.e., the left end of the pseudoplateau region, increases with increasing number of FMA units. In Fig. 4, the limiting brush area of the different triblock copolymer systems was plotted vs the number of FMA units. For both triblock copolymer systems, the area per monomer obtained from the slope of a linear fit is 53.3 Å^2 in $PEO_{10}K$ and 52.2 Å^2 in $PEO_{20}K$ systems. This value agrees well with the value of 52 Å^2 found in the literature for fluorinated amphiphilic molecules [41]. The offset of the linear fit of $PEO_{10}K$ systems equals zero. This implies that the anchored PEO chains can be compressed into a densely packed brush state at the end of the pancake-to-brush transition, which is just hindered by the perfluorinated alkyl layer. In contrast, the offset obtained from the linear fit of the $PEO_{20}K$ systems is 104 Å^2. This is significantly higher than the cross-sectional area (30–40 Å^2) required for two neighbored EO units (the diameter of an EO monomer is 4.5 Å [7]). At this mean molecular area, a putative loop structure can be expected for the PEO block within the subphase. This shows that the PEO block in the $PEO_{20}K$ system is too long to be compressed into a densely packed brush state at the end of the pancake-to-brush transition, even for a vanishing hydrophobic anchor. Most probably, this is due to entropic repulsion between the PEO chains. A further increase in the surface pressure is needed to overcome this. These interpretations are confirmed by comparing the areas for the $PEO_{10}K$ and $PEO_{20}K$ systems at ~65 mN m^{-1}, the collapse pressure. The corresponding mmA are ~56 Å^2 and~90 Å^2, respec-

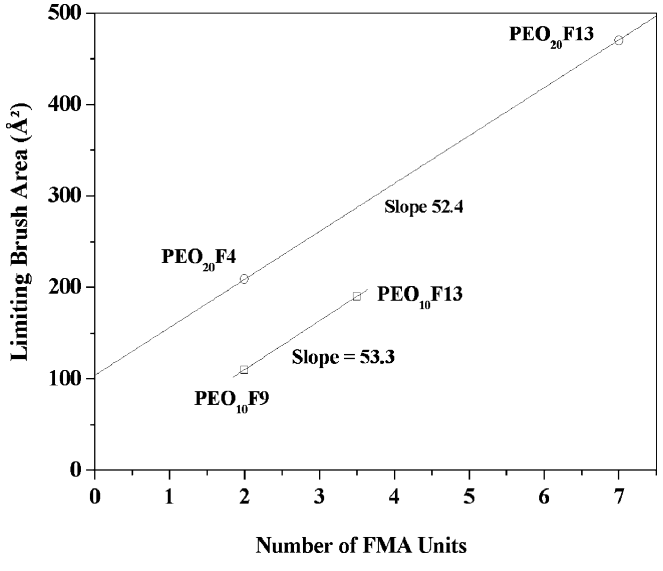

Fig. 4 Limiting brush area over the number of FMA units in the respective block copolymers

tively. For $PEO_{10}K$, this is roughly twice the cross-sectional area for looped PEO chains and similar to the area required for two FMA units in a highly condensed state [41]. Thus, the PEO block indeed is short enough to be compressed into a dense brush state. In contrast, the mmA at the collapse for $PEO_{20}K$ is higher and close to the offset from Fig. 4. This confirms that the longer PEO block in the $PEO_{20}K$ system counteracts the compression. Additionally, it shows that even for the copolymers with low FMA content, dissolution into the subphase is unlikely; they are well anchored at the air–water interface.

A second pseudoplateau or a kink occurs in the brush regime. The surface pressure at the inflection point of the plateau (Table 2) depends on the number of FMA units but is independent from the length of the PEO chain. For $PEO_{10}F_{13}$ and $PEO_{20}F_9$ with nearly the same number of FMA units, the plateau in the brush regime is observed at a surface pressure of approximately 47 mN m^{-1} at slightly different mmA. If this mmA is divided by the number of FMA units per PEO chain, as received from ^{1}H NMR data (Table 2), the resulting areas are around 30 $Å^2$ for one perfluorinated *n*-hexyl side chain in the corresponding triblock copolymer. This is in good agreement with the reported cross-sectional area of 32 $Å^2$ per fluorocarbon side chain [41, 42]. This suggests that the plateau indicates a phase transition within the perfluorinated alkyl chain layer to a closely packed FMA layer. Upon further compression, the surface pressure increases more smoothly until the monolayer collapses. This might come from a rearrangement of the methacrylate backbone as has been reported in lipopolymer systems with very low PEO content [43].

A similar transition is observed in the brush region of different telechelic PEO copolymers [25]. This transition was attributed to the dissolution of the surface-attached alkyl chains resulting in loss of polymer into the subphase. This effect should be the more pronounced, the lower is the content of PFMA in the block copolymers, in opposite to our observations. This is indeed in contrast to our observations. Moreover, the expansion isotherms also show the phase transition in the brush regime, like for compression. Therefore, dissolution of the surface-attached alkyl chains into the subphase cannot account for the transitions we observed.

The phase transition can be either due to crystallization of perfluorinated *n*-hexyl side chains as observed in monolayers of perfluorinated amphiphiles [41] or due to the rearrangement of PFMA blocks at the air–water interface. Atsuhiro et al. [41] observed a similar phase transition in isotherms of amphiphilic 2-(perfluorodecyl) ethyl methacrylate. It was interpreted as the result of crystallization of perfluorinated chains at higher surface pressure. The isotherms were not reversible due to crystallization. In contrast, our isotherms of PEO-PFMA triblock copolymers show reversibility. Thus, a crystallization of perfluorinated *n*-hexyl side chains is unlikely in this study. With increasing PFMA content, the second phase transition becomes more significant and is observed as a pronounced plateau in isotherms of $PEO_{20}F_{69}$ copolymer [44]. A close analysis of the second phase transition observed in this high PFMA content copolymer reveals that the plateau corresponds to both, the condensation of fluorinated alkyl chains and rearrangement of PFMA block. In $PEO_{20}F_{13}$ copolymer isotherm, the second phase transition begins at 285 $Å^2$ mmA which is higher than the area required for closely packed FMA units in the copolymer (7×32 $Å^2$=224 $Å^2$) and ends at ~140 $Å^2$ mmA, which is smaller. Thus, with increasing FMA content, a combination of condensation of FMA units and rearrangement of PFMA block might reflect the second phase transition. The minimum areas to which the monolayers can be compressed further support our assumption that a vertical rearrangement of PFMA block takes place at low mmA. The block copolymers with at least three to four FMA units show a collapse area, which is lower than that for densely packed FMA units. Thus, a rearrangement of the FMA units must occur before the collapse. In contrast, the copolymers with a low PFMA content collapse at an area, which is the same or bigger than that for a densely

Table 2 Different characteristic values of copolymers

Copolymer	M_n[a] (g mol^{-1})	*n*(EO)[b]	*n*(FMA)[c]	MMA_{ob}[d] ($Å^2$)	MMA_{spt}[e] ($Å^2$)
$PEO_{10}F_9$	10,890	227	2	110	
$PEO_{10}F_{13}$	11,490	227	3–4	190	101
$PEO_{20}F_4$	20,834	455	2	209	
$PEO_{20}F_9$	21,978	455	4–5	230	133
$PEO_{20}F_{13}$	22,988	455	7	470	270

[a]The molar mass was calculated based on ^{1}H NMR data, e.g., from Table 1. It is known that $PEO_{10}F_9$ contains 9 wt% of PFMA block and 91 wt% of PEO block. The molar masses of PEO blocks in $PEO_{10}K$ and $PEO_{20}K$ systems were taken as 10,000 and 20,000 g mol^{-1}, respectively. From these data, molar masses of triblock copolymers were calculated and used for Langmuir monolayer measurements
[b]The number of EO units is calculated by dividing the molar mass of PEO in the copolymers with the EO molar mass
[c]The PFMA block mass was calculated by deducting the PEO block mass from the overall block copolymer molar mass. The molar mass of a single FMA unit was taken as 432 g mol^{-1} to calculate the number of FMA units
[d]Limiting brush area per molecule
[e]Mean molecular area corresponding to the inflection point in the second phase transition

packed FMA layer. Thus, rearrangement of PFMA block is not likely in these systems.

Morphology of the Langmuir–Blodgett films

A monolayer of $PEO_{10}F_{13}$ copolymer was transferred at different surface pressures, 0.5, 3, 20, and 35 mN m^{-1}, onto the silicon substrates by the LB technique. These surface pressures were chosen based on the plateaus observed in the monolayer, indicating a change in the copolymer organization at the air–water interface, i.e., a phase transition. The transfer efficiency of the LB films can be measured by the transfer ratio. It is defined as the ratio of the area of monolayer removed from the air–water interface to that of the substrate to be deposited. In case of low molecular weight amphiphilic molecules, it was found that the transfer ratio should be equal to 1 [4]. In our triblock copolymer system, the LB films were transferred with high transfer ratios of 1.5 and 1.3 at 0.5 and 3 mN m^{-1}, respectively. In the brush regime (at high surface pressures 20 and 35 mN m^{-1}), they were transferred with a transfer ratio of 1.

Figure 5a shows an AFM image of a $PEO_{10}F_{13}$ LB film transferred at 0.5 mN m^{-1} with the corresponding 3D image (Fig. 5b). A very thin layer (<4 nm) with elevated white appearing spots is observed in Fig. 5a. A zoom-in into Fig 5a shows small domain structures projected toward the air–water interface in the size range of 50–100 nm. The height of these domains varies between 1.5 and 3 nm. The height of the domains is larger than a monolayer thickness, which implies an aggregation of the triblock copolymer. Overall, the size of these domains is consistent with 2D micelles observed in LB film studies of PS-*b*-PEO by Zhu et al. [26–30] and Logan et al. [22, 23]. They have observed micelle structures with elevated, white appearing PS cores above a dark appearing PEO corona. Due to the hydrophilic nature of silicon surfaces, the PEO block is oriented toward the silicon substrates, and both silicon substrate and PEO repel the PFMA block. This repulsion leads to aggregation. Thus, the entire domain, as observed in Fig. 5b, illustrates a micellar structure with a PEO corona and PFMA blocks anchoring toward air–copolymer interface. Thus, higher elevated parts of these domains can be assigned to PFMA. At this surface pressure, the isotherms are similar to the PEO homopolymer isotherms in which isolated pancakes are expected. Because 3D micelles do not exist at the air–water interface, they must be formed during or after film transfer.

Figure 6a shows the morphology of the LB films of $PEO_{10}F_{13}$ transferred at a surface pressure of 3 mN m^{-1}. The size of the surface micelles is similar to the size observed at the lower surface pressure of 0.5 mN m^{-1}. In contrast, the height of the domain structures is considerably increased to 3–5 nm (see Fig. 6b). This can be assigned to stretching of PEO molecules into the water subphase upon compression before transfer.

Figure 7a shows the AFM image of the LB film morphology of $PEO_{10}F_{13}$ transferred at a surface pressure of 20 mN m^{-1}. It shows a finger-like morphology typical for crystallized PEO homopolymer monolayers in thin spin-coated films [45–47]. They are formed due to the conformational difference between the PEO chains adsorbed on the silicon surface and the chains that are not adsorbed [45–47]. This morphology can only be observed if the film is thick enough or only after significant supercooling to overcome the nucleation barrier [48]. Thus, we observe it only at a higher surface pressure, where the monolayer is in a condensed state with densely packed

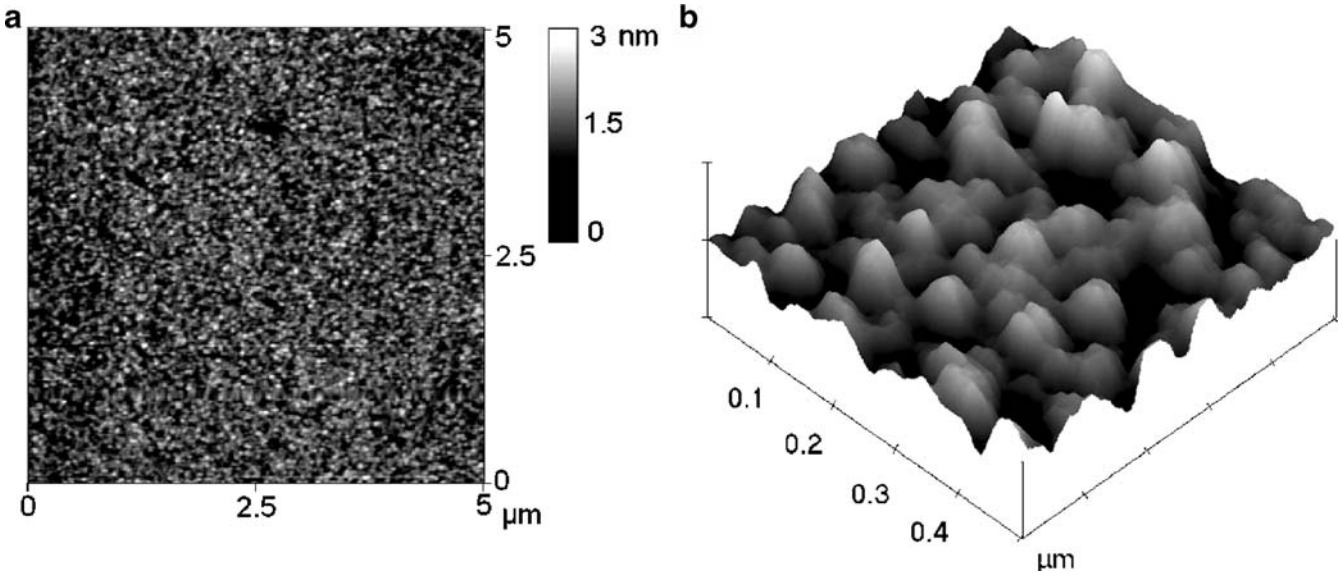

Fig. 5 **a** AFM image of the $PEO_{10}F_{13}$ triblock copolymer transferred at surface pressure of 0.5 mN m^{-1}. **b** Corresponding 3D AFM image of $PEO_{10}F_{13}$ triblock copolymer. Surface micelles projected toward the surface can clearly be seen

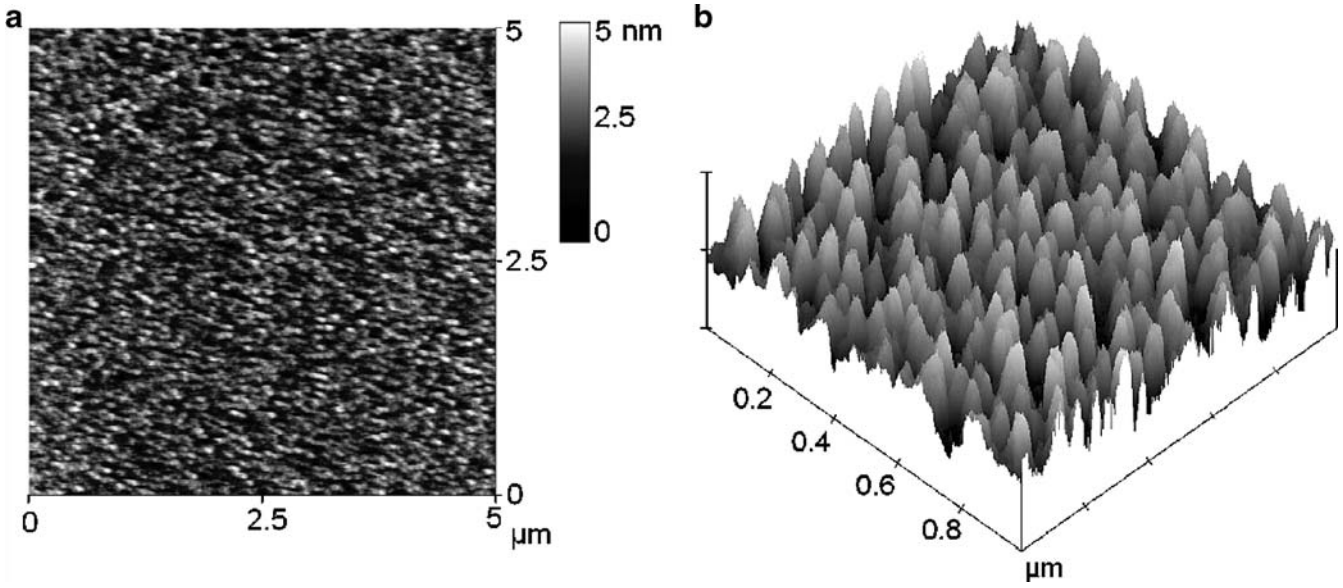

Fig. 6 **a** AFM image of the $PEO_{10}F_{13}$ triblock copolymer transferred at a surface pressure of 3 mN m^{-1}. **b** Corresponding 3D AFM image of $PEO_{10}F_{13}$ triblock copolymer. Surface micelles in the range of 50–100 nm size projected toward the surface are clearly visible

brushes and thus thick enough. Moreover, the $PEO_{10}F_{13}$ copolymer contains three to four FMA units, and the volume content of PFMA in $PEO_{10}F_{13}$ copolymer is only 10 vol.%. This is very small compared to the volume fraction of the PEO block (the densities of 1.22 g cm^{-3} for PEO and 1.69 g cm^{-3} for PFMA are measured in a helium pycnometer). Thus, the PFMA blocks have less effect on the PEO conformation on the silicon surface, and the crystallization of PEO chains is not hindered. Figure 7b shows a zoom-in into the transferred monolayer. Irregular domains with heights between 2 and 4 nm are visible between the finger-like patterns. This observation is in agreement with the assumption that upon transfer, a monolayer covers the entire surface area of the silicon wafer. It further supports the assumption that the finger-like patterns are developed due to crystallization of the block copolymers after the film transfer.

Figure 8a shows an AFM image of LB film morphology of $PEO_{10}F_{13}$ transferred at 35 mN m^{-1}. The surface area covered by the finger-like morphology is increased compared to the LB film morphology obtained at 20 mN m^{-1}. A closer look at these finger-like patterns reveals

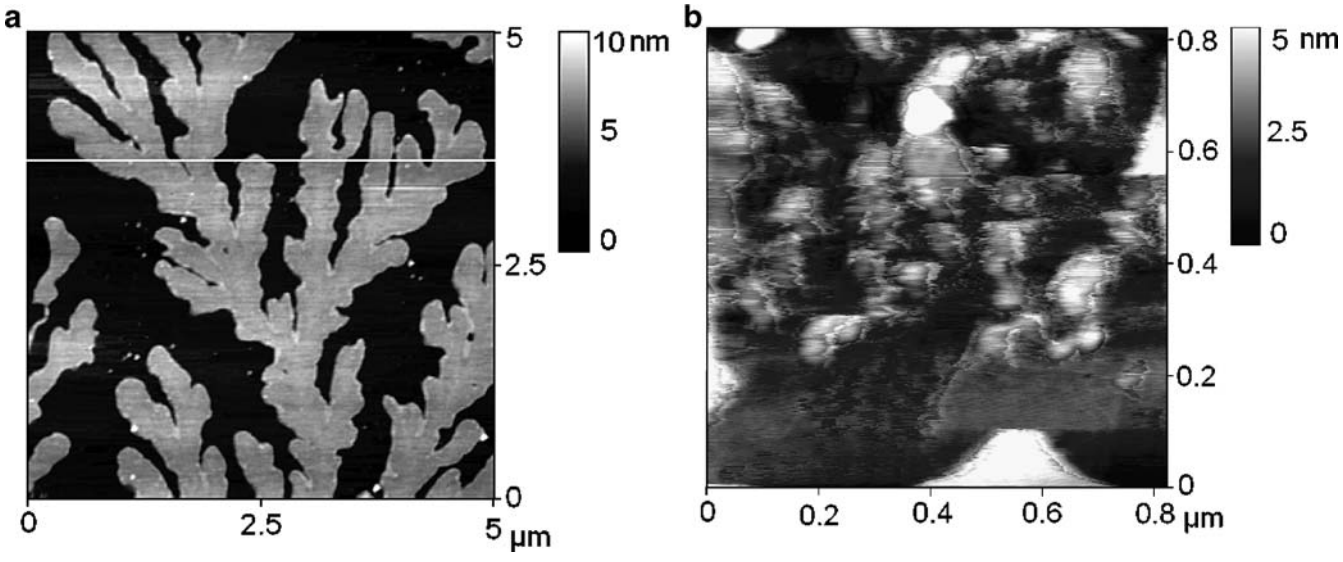

Fig. 7 **a** AFM image of the $PEO_{10}F_{13}$ triblock copolymer at a surface pressure of 20 mN m^{-1}. **b** Zoom-in into the space between the finger-like patterns from Fig. 7a. Irregularly shaped aggregates are observed

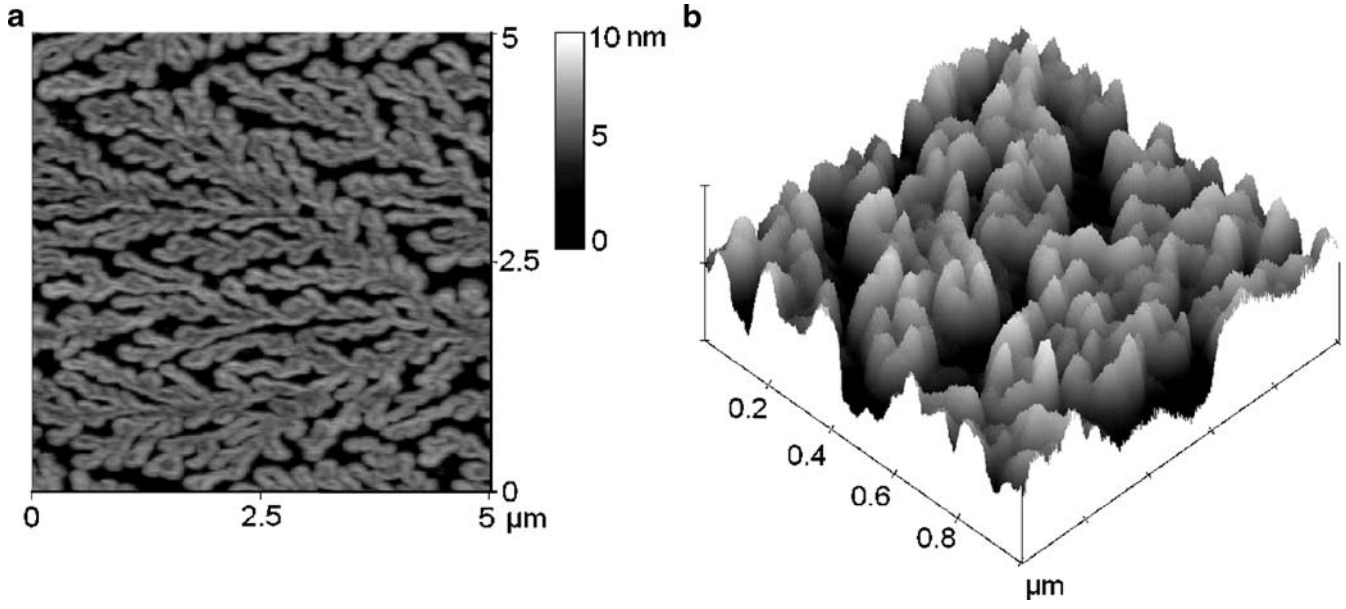

Fig. 8 **a** AFM image of the $PEO_{10}F_{13}$ triblock copolymer transferred at a surface pressure of 35 mN m^{-1}. **b** Zoom-in into the finger-like patterns in Fig 8a. Finger-like patterns are composed of surface micelles similar to that observed at lower surface pressures

that these structures are composed of densely packed surface micelles as can be seen in the 3D AFM image (Fig. 8b). These surface micelles are projected toward the surface, with similar size range as observed in Fig. 6b. This further supports our assumption that the formation of 3D micelles and of finger-like structures occurs during or after the transfer to the silicon substrate.

Figures 9 and 10 show AFM images of $PEO_{20}F_4$ and $PEO_{20}F_{13}$ copolymer LB films transferred at 20 and 35 mN m^{-1}, respectively. Again, finger-like patterns are observed for $PEO_{20}F_4$ at both surface pressures with increasing density. Compared to $PEO_{20}F_4$ LB film, the crystallization of PEO is hindered in the $PEO_{20}F_{13}$ copolymer LB film transferred at 20 mN m^{-1} (Fig 10a) or even missing at 35 mN m^{-1} (Fig. 10b). This indicates that the PFMA content in $PEO_{20}F_{13}$ is high enough to suppress the crystallization of PEO, as was discussed for bulk crystallization of block copolymers [38]. To discuss the role of the PEO middle block in detail, the AFM images of $PEO_{10}F_{13}$ and $PEO_{20}F_4$ LB films at surface pressure 20 mN m^{-1} are compared.

Figure 11 shows the height profile of the LB films shown in Fig. 7a and Fig. 9a taken along the indicated lines. The height of the fingers is 3.8 nm for $PEO_{10}F_9$ and 6.5 nm $PEO_{20}F_4$. The increase in the height of the fingers for

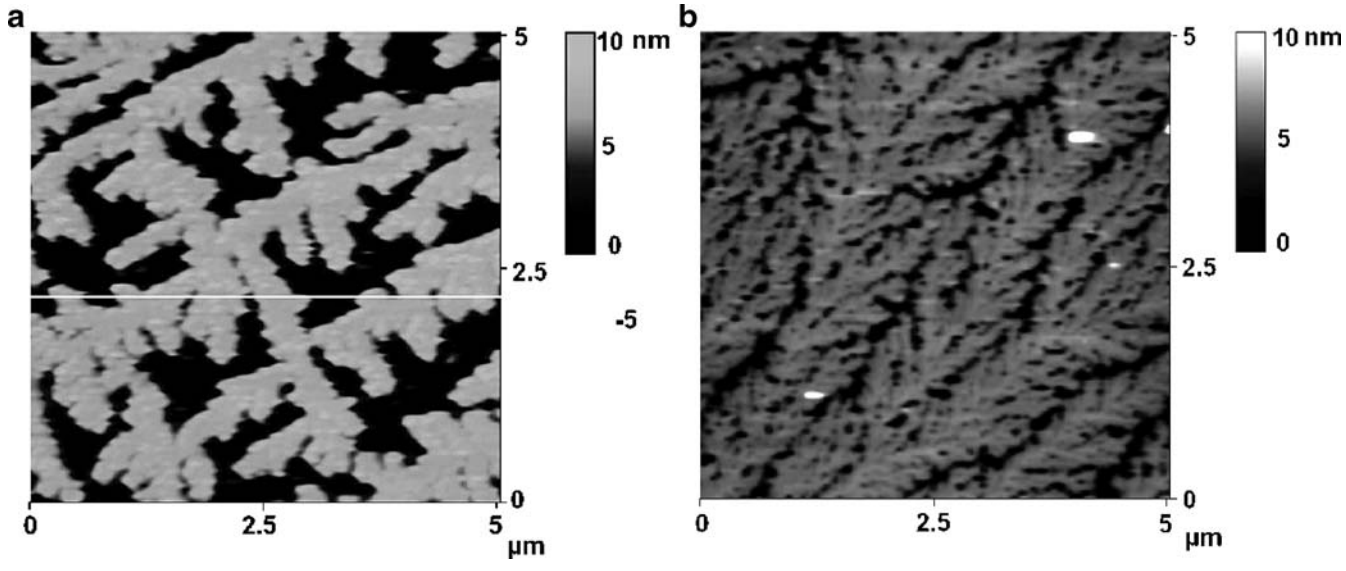

Fig. 9 AFM image of the $PEO_{20}F_4$ triblock copolymer transferred at surface pressures of **a** 20 mN m^{-1} and **b** 35 mN m^{-1}

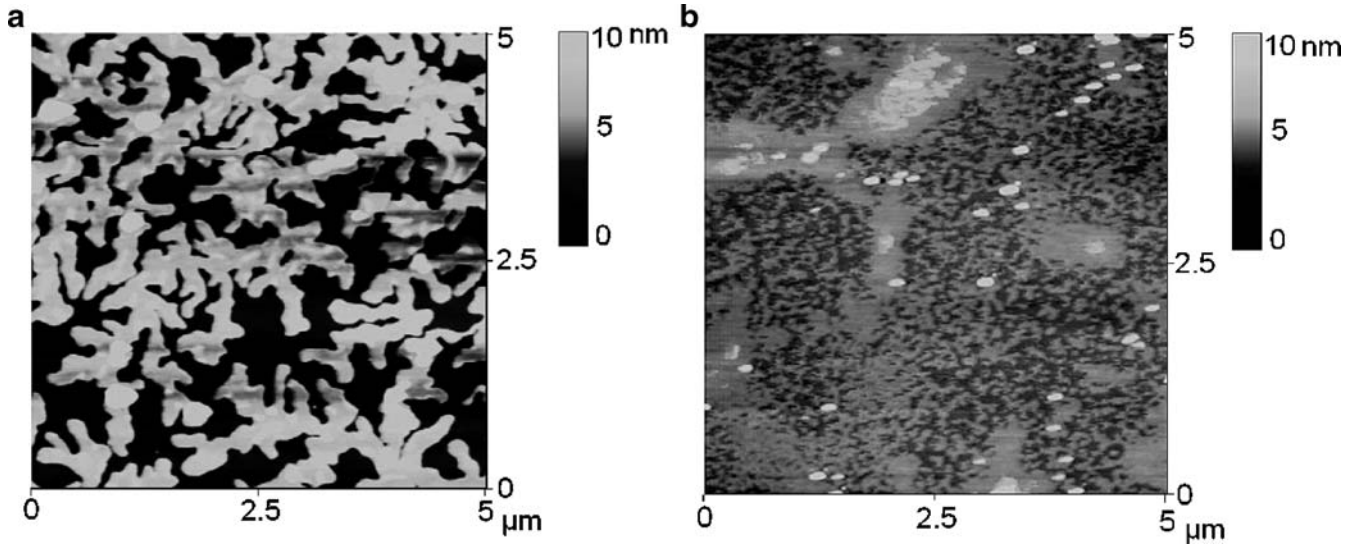

Fig. 10 AFM image of the $PEO_{20}F_{13}$ triblock copolymer transferred at a surface pressures of **a** 20 mN m^{-1} and **b** 35 mN m^{-1}

$PEO_{20}K$ copolymer can be related to the higher molar masses of the PEO middle block. According to Reiter and coworkers [45–47], the thickness or height of the fingers gives information about chain folding and thus about organization of polymer segments in the crystal. In our LB films, the height of the finger-like patterns is significantly lower when compared to a fully stretched molecule. For instance, the lengths (L) of fully stretched crystalline $PEO_{10}K$ and $PEO_{20}K$ molecules are 63 and 125 nm, respectively [L=0.2783 nm × (M_n^{PEO}/M_n^{EO})=63 nm] (0.2783 nm is the ethylene oxide unit length) [49]. This implies that polymer molecules are folded several times due to crystallization. These observations are in accordance with the observations by Reiter and coworkers [45–47].

Figure 12 illustrates the molecular behavior of triblock copolymers with increasing surface pressure in the brush regime. At the limiting brush area (Fig. 12a), the PEO block extends into the subphase forming brushes, anchored by loosely packed PFMA blocks (overlapping region of PFMA blocks). Upon compression (Fig. 12b), at the inflection point of the phase transition in the brush regime, closely packed PFMA blocks are arranged with vertically oriented perfluoro *n*-hexyl ethyl side chains attached to the methacrylate backbone. Near the collapse (Fig. 12c), the whole PFMA blocks are arranged perpendicular to the aqueous subphase.

Conclusions

Amphiphilic triblock copolymers of PEO and PFMA form stable monolayers at air–water interface. It is observed that a small PFMA content (less than 13 wt% of the copolymer) can influence the brush formation of the PEO block. An extended plateau for all copolymers shows the typical phase transition from pancake to brush for the PEO chains. An additional plateau in the brush regime is attributed to rearrangement of PFMA blocks from horizontal to vertical arrangement. The mean molecular area at the second plateau corresponds to the area of closely packed perfluorinated *n*-hexyl side chains of FMA block in the corresponding triblock copolymer system. Therefore, vertically oriented perfluorohexylethyl side chains can be assumed (i.e., methacrylate backbone is arranged horizon-

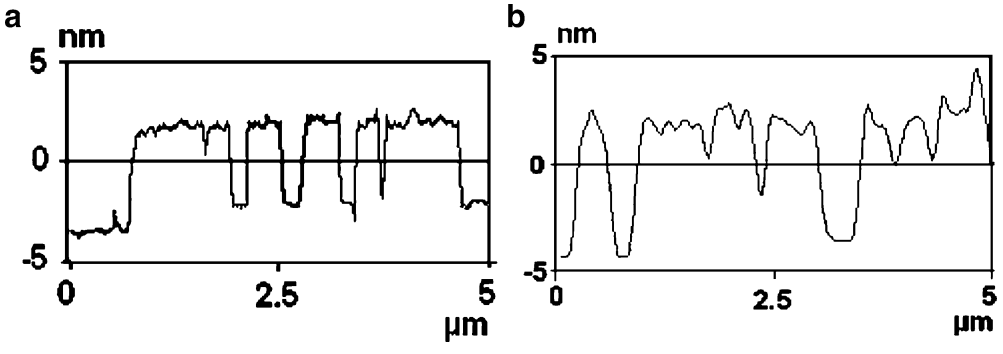

Fig. 11 **a** Height profile of $PEO_{10}F_{13}$ copolymer film shown in Fig. 7a. **b** Height profile of $PEO_{20}F_4$ copolymer film shown in Fig. 9a. These height profiles are taken along the *white lines* in the respective figures

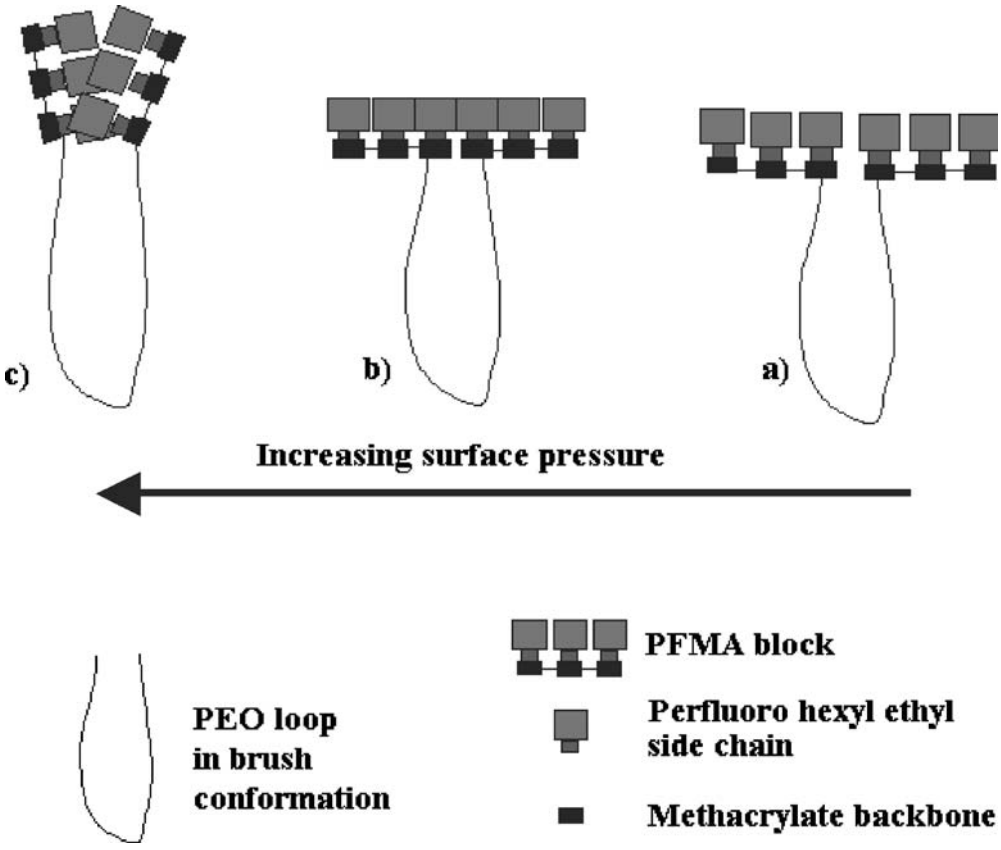

Fig. 12 Schematic representation of triblock copolymer monolayer behavior at air–water interface

tally to aqueous subphase). Upon compression, the whole PFMA block is rearranged perpendicular to the aqueous subphase. LB films transferred at low surface pressure show surface micelles. Triblock copolymer LB films with low PFMA content transferred at high surface pressure show a typical crystalline morphology of PEO. This crystallization was hindered with increasing amount of PFMA content.

In this work, we have studied the monolayer properties of triblock copolymers with a PEO middle block at the air–water interface. Compared to the simple telechelic systems with nonfluorinated alkyl hydrophobic anchoring groups, fluorinated alkyl hydrophobic groups can anchor PEO more strongly at the air–water interface. Additionally, it is an ideal system to study the role of the length of PEO middle blocks on the phase transition within the hydrophobic anchor group. With single anchoring groups at each end of the copolymer, a rearrangement of anchoring group is impossible and the telechelic block copolymers behave like ordinary anchored PEO chains. In contrast, a rearrangement within the anchor groups is probable with an increasing number of anchoring groups (greater than or equal to three FMA units). The packing density of the anchoring groups also depends on the length of the middle block. $PEO_{10}K$ systems with 227 EO units form nearly dense brushes with molecular area of 56 $Å^2$. For the longer $PEO_{20}K$ systems with 455 EO units, the minimum area is 90 $Å^2$. Thus, the cross-sectional area of the hydrophobic anchor groups has to be larger than these limiting areas for a rearrangement of the anchor groups to be possible.

Acknowledgements The support from SFB 418 and DFG is acknowledged. We thank Dr. Hesse for allowing us to use the AFM instrument and to Dr. Alexe for his technical assistance (Max Planck Institute for Microstructure Physics, Halle).

References

1. Xu R, Winnik MA, Hallett FR, Riess G, Croucher MD (1991) Macromolecules 24:87
2. Tuzar Z, Kratochvil P (1976) Adv Colloid Interface Sci 6:201
3. Koutsos V, van der Vegte EW, Pelletier E, Stamouli A, Hadziioannou G (1997) Macromolecules 30:4719
4. Ulman A (1991) An introduction to ultrathin organic films from Langmuir–Blodgett to self-assembly. Academic, New York
5. Goncalves da Silva AM, Filipe EJM, Oliveira JMR, Martinho JMG (1996) Langmuir 12:6547
6. Sauer BB, Yu H, Tien CF, Hager DF (1987) Macromolecules 20:393
7. Goncalves da Silva AM, Filipe EJM (1996) Langmuir 12:6547

8. Gragson DE, Jensen JM, Baker SM (1999) Langmuir 15:6127
9. Faure MC, Bassereau P, Carignano MA, Szleifer I, Gallo Y, Andelman D (1998) Eur Phys J B 3:365
10. Faure MC, Bassereau P, Lee LT, Menelle A, Lheveder C (1999) Macromolecules 32:8538
11. Goncalves da Silva AM, Simoes Gamboa AL, Martinho JMG (1998) Langmuir 14:5327
12. Dewhurst PF, Lovell MR, Jones JL, Richards RW, Webster JRP (1998) Macromolecules 31:7851
13. Robert BC, Matthew GM (2005) Langmuir 21:5453
14. Bijsterbosch HD, de Haan VO, de Graaf AW, Mellema M, Leermakers FAM, Cohen Stuart MA, van Well AA (1995) Langmuir 11:4467
15. Baker SM, Leach KA, Devereaux CE, Gragson DE (2000) Macromolecules 33:5432
16. Cox JK, Constantino B, Yu K, Eisenberg A, Lennox RB (1999) Langmuir 5:7714
17. Gragson DE, Jacob MJ, Baker SM (1999) Langmuir 15:6127
18. Devereaux CA, Baker SM (2002) Macromolecules 35:1921
19. Cox JK, Yu K, Eisenberg A, Lennox RB (1999) Phys Chem Chem Phys 18:4417
20. Raju F, Andrew MS, Stephen RC, Jennifer LL, Royale SU, Stephanie ADT, Yves G, Randolph SD (2002) Macromolecules 35:6483
21. Peleshanko S, Jeong J, Gunawidjaja R, Tsukruk VV (2004) Macromolecules 37:6511
22. Logan JL, Pascal M, Brian D, Andrew MS, Sergei SS, Raju F, Daniel T, Yves G, Randolph SD (2005) Langmuir 21:3424
23. Logan JL, Pascal M, Daniel T, Yves G, Randolph SD (2005) Langmuir 21:7380
24. Alexander S (1977) J Phys 38:983
25. Barentin C, Muller P, Joanny JF (1998) Macromolecules 31:2198
26. Zhu J, Eisenberg A, Lennox RB (1991) Langmuir 7:1579
27. Zhu J, Eisenberg A, Lennox RB (1991) J Am Chem Soc 113:5583
28. Zhu J, Eisenberg A, Lennox RB (1992) J Phys Chem 96:4727
29. Zhu J, Eisenberg A, Lennox RB (1992) Macromolecules 25:6547
30. Zhu J, Eisenberg A, Lennox RB (1992) Macromolecules 25:6556
31. Li S, Hanley S, Khan I, Eisenberg A, Lennox RB (1993) Langmuir 9:2243
32. Li Z, Zhao W, Quinn J, Rafailovich MH, Sokolov J, Lennox RB, Eisenberg A, Wu XZ, Kim MW, Sinha SK, Tolan M (1995) Langmuir 11:4785
33. Li S, Clarke CJ, Lennox RB, Eisenberg A (1998) Colloids Surf 133:191
34. Karim A, Slawecki TM, Kumar SK, Douglas JF, Satija SK, Han CC, Russell TP, Liu Y, Overney R, Sokolov J, Rafailovich MH (1998) Macromolecules 31:857
35. An SW, Su TJ, Thomas RK, Baines FL, Billingham NC, Armes SP, Penfold J (1998) J Phys Chem B 102:387
36. Israelachvili J (1994) Langmuir 10:3774
37. Hussain H, Busse K, Kressler J (2003) Macromol Chem Phys 204:936
38. Hussain H, Kerth A, Blume A, Kressler J (2004) J Phys Chem B 108:9962
39. Hussain H, Budde H, Höring S, Busse K, Kressler J (2002) Macromol Chem Phys 203:2103
40. Chunhung W, Tianbo L, Henry W, Benjamin C (2000) Langmuir 16:656
41. Atsuhiro F, Tohru A, Hiro N (2002) J Colloid Interface Sci 247:351
42. Aminuzzaman M, Kado Y, Mitsuishi M, Miyashita T (2003) Polymer J 35:785
43. Kuhl TL, Majewski J, Howes PB, Kjaer K, von Nahmen A, Lee K YC, Ocko B, Israelachvilli JN, Smith GS (1999) J Am Chem Soc 121:7682
44. Chiranjeevi P, Busse K, Kressler J (2006) (Manuscript in preparation)
45. Reiter G, Sommer JU (2000) J Chem Phys 112:4376
46. Reiter G, Sommer JU (2000) J Chem Phys 112:4384
47. Reiter G (2003) J Poly Sci 41:1869
48. Reiter G, Castelein G, Sommer JU, Röttele A, Thurn-Albrecht T (2001) Phys Rev Lett 87:226101
49. Kovacs AJ, Straupe C (1980) J Cryst Growth 48:210